第 49 卷 第 8 期/2022 年 4 月/中国激光 研究论文

中国激光

车轴激光清洗表面质量分析及在线评估

王春生[1]，王洪潇[1]，徐惠妍[2]，何广忠[1]，李凯[1]，谷晓鹏[2]，董娟[2*]

[1]中车长春轨道客车股份有限公司工程技术中心，吉林 长春 130113；

[2]吉林大学材料科学与工程学院，吉林 长春 130112

摘要 基于高铁转向架轮对在高级检修过程中的漆层去除需求，采用激光清洗技术对高强钢表面漆层进行去除，研究不同功率下漆膜的去除状况，分析不同清洗状态下工件表面的宏观、微观形貌及成分变化；之后，采用机器视觉技术提取工件表面状态图像并进行处理，提取出黑、白像素点的差异并将其作为特征值对工件表面的清洗状态进行判定，为高强钢表面漆层的去除提供了实用的工艺参数及检测方法。

关键词 激光技术；激光清洗；表面形貌；激光测距；在线评估

中图分类号 TG178 **文献标志码** A **doi**：10.3788/CJL202249.0802005

1 引 言

转向架轮对作为高铁的主要部件，具有极为严格的检修要求，在高级检修过程中需要对其进行磁粉探伤[1-2]。在车轴探伤之前，需要去除轴身部分的涂层。传统的表面涂层去除方法为机械打磨和化学处理，即：首先采用化学处理进行脱漆，然后在未除净的局部区域用布砂轮进行打磨去除[3-4]。在布砂轮打磨工序中，由于残余漆膜分布不均匀且随机性较强，因此需要采用人工进行选区打磨，但这易导致局部区域过度打磨，进而造成表面损伤[5]。当损伤较深时，必须更换车轴。因此，亟需开发出一种全新的脱涂层技术，以减少环境污染、降低人力成本，实现绿色、高效高质的涂层去除。

激光清洗技术具有清洗精度高、无需使用化学清洗剂、无物理机械接触、可达性好、便于实现自动化等优势[6]，在表面除漆（或除锈除污渍）、模具清洗、晶体表面处理等领域得到了广泛应用[7]。目前，激光除漆技术的研究主要集中在铝合金[8-9]、管线钢[10]、灰铸铁[11]等基材表面，而不同的基材对激光清洗效果有不同的影响。前人的研究表明：在激光除漆过程中，当激光输入低于阈值条件时，漆层在振动效应的作用下剥离；当激光输入高于阈值条件时，基材在振动效应和烧蚀效应的综合作用下会出现一定损伤[12-13]。因此，在实际的工程应用中，激光清洗阈值是极为关键的工艺参数。目前，对工件表面激光清洗效果的评估方法主要包括三种：1）基于发射光谱特征的光信号检测[14]；2）基于声波强度变化的声信号检测[15-17]；3）基于图像处理技术的机器视觉检测[18-19]。其中的机器视觉检测技术由于具有成本较低、抗环境干扰能力强等优势，成为了新兴的发展方向。本研究团队针对现有高铁转向架轮对车轴轴身涂层激光清洗去除的工艺需求，开展了高强钢表面涂层激光清洗工艺分析、激光清洗后高强钢表面微结构演变、激光清洗后表面质量在线评估方法的研究，以期为高铁车身关键零部件的绿色高效表面处理技术提供参考。

2 试验方法

试验板材为车轴部件用高强钢，其表面形貌如图 1(a)所示。成分分析表明，试验用高强钢表面有一层氧化膜。在试样表面喷涂枣红色底漆和灰色面漆，其中底漆厚度为 50～60 μm，面漆厚度为 230～260 μm。图 1 所示为工件喷漆前及喷漆后的表面形貌。

收稿日期：2021-07-29；**修回日期**：2021-08-24；**录用日期**：2021-09-22

基金项目：国家重点研发计划（2017YFB1105000）、吉林省科技发展计划（20190302044GX）、长春市科技计划（18SS016）

通信作者：*dongjuan@jlu.edu.cn

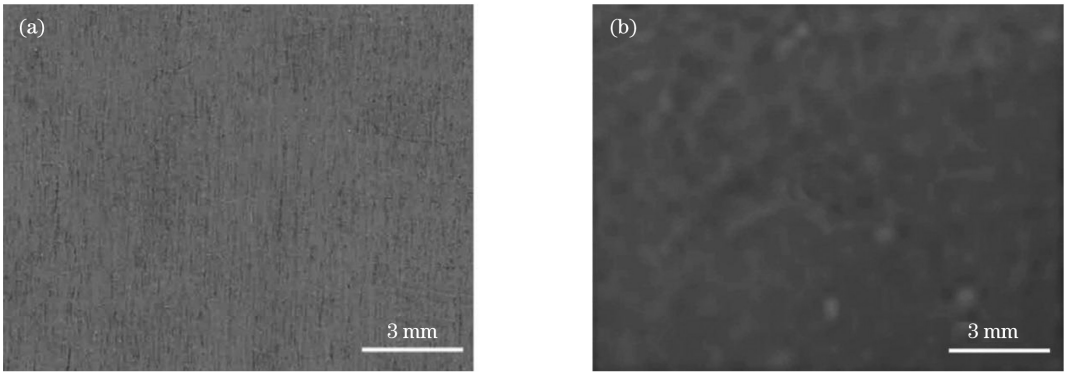

图 1 试样喷漆前后的表面形貌对比。(a)喷漆前;(b)喷漆后

Fig. 1 Surface morphology comparison of sample before and after painting. (a) Before painting; (b) after painting

激光清洗试验装置为德国 IPG 公司生产的 1064 nm 纳秒脉冲光纤激光清洗系统,其基本结构如图 2 所示。纳秒脉冲激光除漆系统的主要技术参数如表 1 所示。

进行激光清洗试验时,激光沿“弓”字形路径在试样表面进行扫描,如图 3 所示。激光清洗工艺参数如表 2 所示。清洗试验结束后,分别采用激光共聚焦显微镜、数码显微镜、场发射扫描电镜对试样的表面形貌和成分进行观察和分析。

表 1 纳秒脉冲激光器的主要技术参数

Table 1 Main technical parameters of nanosecond pulsed laser

Technical parameter	Value
Maximum and mean power /W	1000,200
Wavelength /μm	1.06
Focus diameter /mm	0.96
Focal length /mm	183,193
Pulse frequency /kHz	2–50,200
Pulse width /ns	30,60,100,120

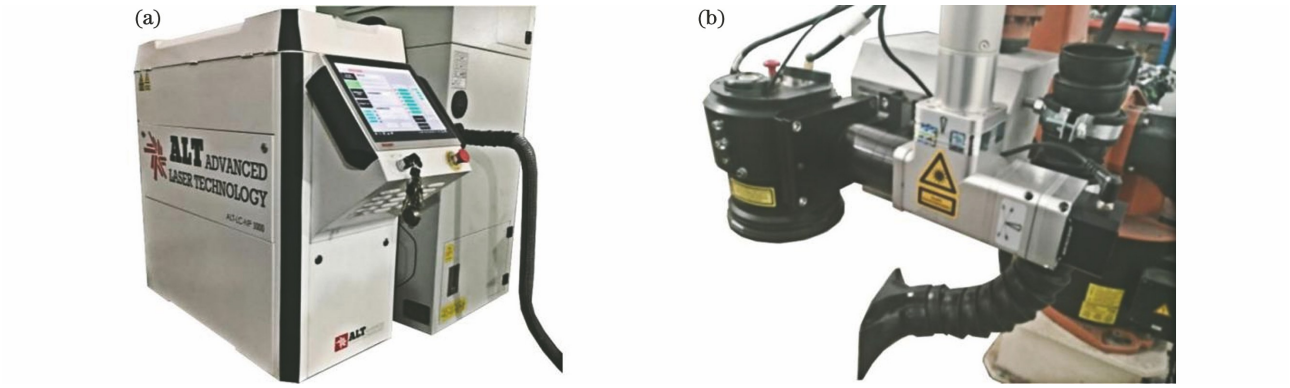

图 2 纳秒脉冲激光清洗设备。(a)脉冲光纤激光器;(b)激光清洗头

Fig. 2 Nanosecond pulsed laser cleaning equipment. (a) Pulsed fiber laser; (b) laser cleaning head

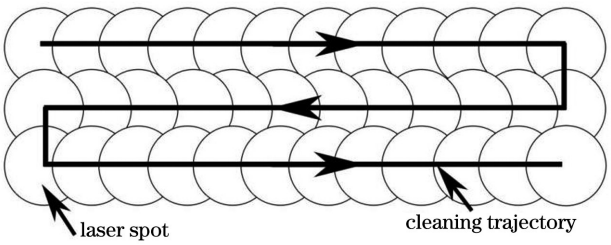

图 3 激光清洗扫描路径示意图

Fig. 3 Schematic of scanning path of laser cleaning

表 2 激光清洗主要工艺参数

Table 2 Main process parameters of laser cleaning

Cleaning parameter	Value
Pulse width /ns	30
Pulse frequency /kHz	30
Laser power /W	70–240 (progressive increase every 10 W)
Scanning length /mm	20
Scanning width /mm	15
Scanning speed /(m·s^{-1})	0.5
Laser lap ratio	0.2

为了结合工件的宏观、微观形貌对激光清洗质量进行在线评估,设计了如图4所示的激光清洗工

件表面检测设备：采用 Y 向精密运动模块带动 Basler 公司的 raL6144-16gm 线阵相机在工件表面进行覆盖式扫查，采集工件的表面信息。

图 4 激光清洗表面在线检测设备

Fig. 4 Online detection mechanism of laser cleaning surface

3 试验结果与讨论

3.1 清洗表面的宏观分析

试样表面的漆层由枣红色底漆和灰色面漆组成，因此通过观察表面宏观形貌可以大致判断清洗效果：表面呈灰色，可认为面漆未清洗完全；表面呈枣红色，可认为面漆清洗干净而底漆未清洗完全；表面呈具有金属光泽的银白色，可认为油漆清洗完全且基材受损较少；表面呈蓝紫色甚至黑色，可认为基材损伤严重。

为了分析激光功率对清洗效果的影响，在不同的激光功率下对试样表面进行清洗，清洗后的表面形貌如图 5 所示。当激光功率为 70 W 时，只能去除部分面漆，表面光滑且为浅灰色；当激光功率为 150 W 时，面漆被去除，试样表面呈枣红色；当激光功率达到 200 W 时，能基本去除漆层，表面呈银白色，在光学显微镜下可观察到表面有沟壑状裂纹；当激光功率为 240 W 时，清洗过度，试样表面呈蓝紫色，表明存在烧蚀现象。可见，随着激光功率增大，漆层去除率逐渐增加，且当激光功率低于 150 W 时，基本不能清除底漆。因此，接下来主要针对 150～240 W 激光功率下清洗的试样表面进行微观形貌分析。

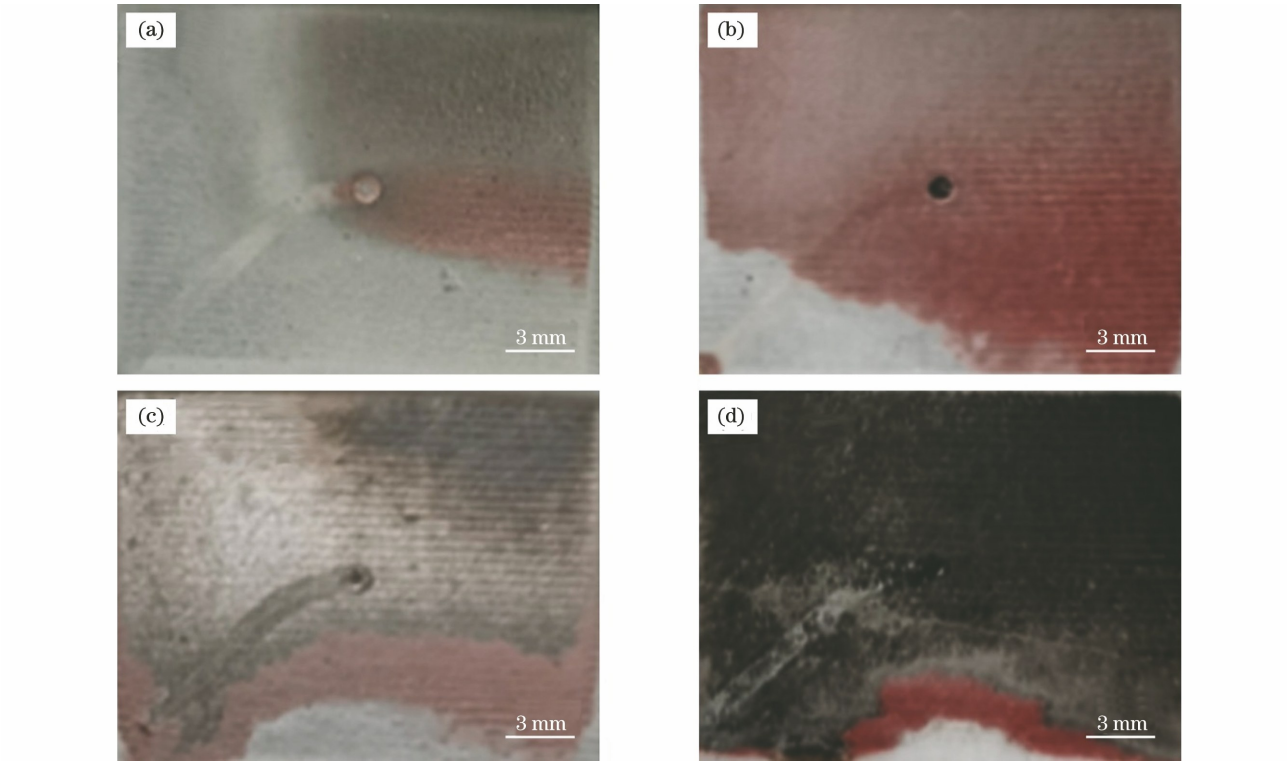

图 5 不同功率下激光清洗后试样表面的宏观形貌。(a)70 W；(b)150 W；(c)200 W；(d)240 W

Fig. 5 Macroscopic appearances of sample surface cleaned by laser with different powers. (a) 70 W; (b) 150 W; (c) 200 W; (d) 240 W

采用激光共聚焦显微镜分析清洗表面的微观形貌，结果如图 6 所示。在 150 W 的低功率下清洗后，表面有平行的沟壑纹路，且表面尚残留较多油漆。这说明该功率下激光清洗不足，激光能量加载较多的直射点处油漆清洗得较干净。此外，清洗表面的沟壑大体沿着激光扫描方向，且沟壑纹理宽度约等于扫描行间距(200 μm)，由此可以判断该纹路是激光清洗扫描过程中导致的。当激光功率增大到 180 W 时，表面较为平整，既无沟壑也无熔坑，说明表面清洗质量良好。当激光功率增大到 200 W 时，表面分布着或大或小的熔坑，说明表面出现了一定的烧蚀。随着激光功率继续增大至 240 W，表面越来越不平整，可知此时基材损伤较重。由以上分析可知，当激光功率增大到 200 W 时，表面已经出现了较为明显的烧蚀现象，因此，后续将重点研究 150～200 W 功率范围内的激光清洗效果。

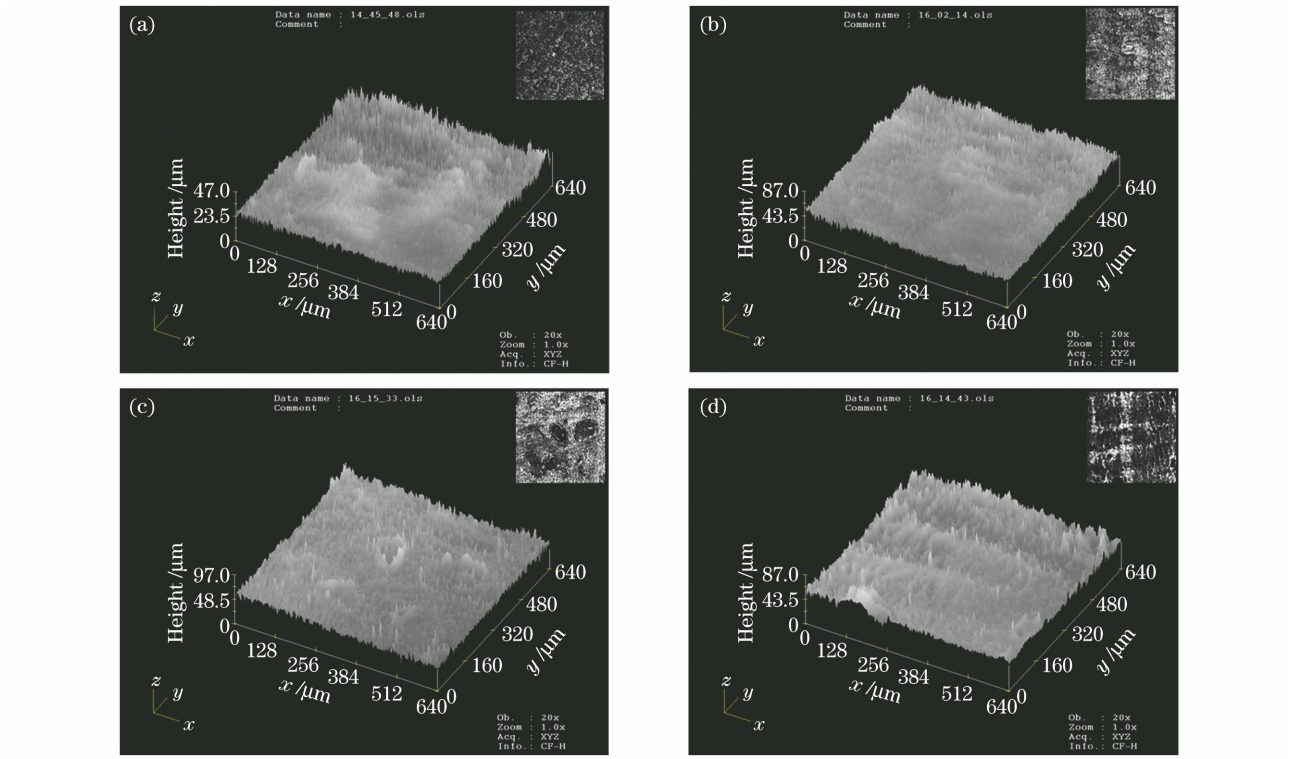

图 6　不同功率下激光清洗后表面微结构的高度云图(频率为 30 kHz)。(a)150 W；(b)180 W；(c)200 W；(d)240 W

Fig. 6　Height cloud images of surface microstructure after laser cleaning at different powers (frequency is 30 kHz). (a) 150 W; (b) 180 W; (c) 200 W; (d) 240 W

3.2　清洗表面的微观形貌

采用数码显微镜对 30 kHz 脉冲频率下不同激光功率清洗后的表面微观形貌进行分析，结果如图 7 所示。当激光功率为 150 W 时，底漆表面无烧焦痕迹，且表面较不平整，可判断剥离机制占主导作用。当激光功率增大到 160 W 时，表面(基材表面的氧化膜)隐约有同向分布裂纹显现，同时表面仍残留有大量的底漆。当激光功率增大至 180 W 时，表面的金属光泽更为明显，表面上几乎没有可见底漆残留，氧化膜上的裂纹更加清晰，但在氧化膜薄弱处，出现了零星的重熔现象。当激光功率增大至 200 W 时，表面无底漆残留，氧化膜裂纹边缘出现了钝化现象，且出现了火山口状重熔形貌，基材出现轻微损伤。

采用扫描电镜对 30 kHz 频率下不同激光功率清洗后的表面形貌进行分析，结果如图 8 所示。当激光功率为 150 W 时，表面的微观形貌如图 8(a)所示，此时的激光功率不足以使基材露出。当激光功率加大至 160 W 时，如图 8(b)所示，漆层上出现了孔洞，且孔洞沿激光扫描路径分布。这是因为扫描路径中心区域的能量高，能将漆层去除干净(露出基材)，而扫描路径边缘能量较低，无法将漆层去除干净。当激光功率增大至 170 W 时，如图 8(c)所示，表面漆层均已去除干净，露出的表面上分布有大量同向微纹，且局部区域出现了凹坑，如图 8(c)中的 A 所示。当激光功率增至 180 W 时，如图 8(d)所示，表面上残留有区域 B 所示的颗粒状物体和区域 C 所示的凹坑。当激光功率增至 190 W 时，如图 8(e)

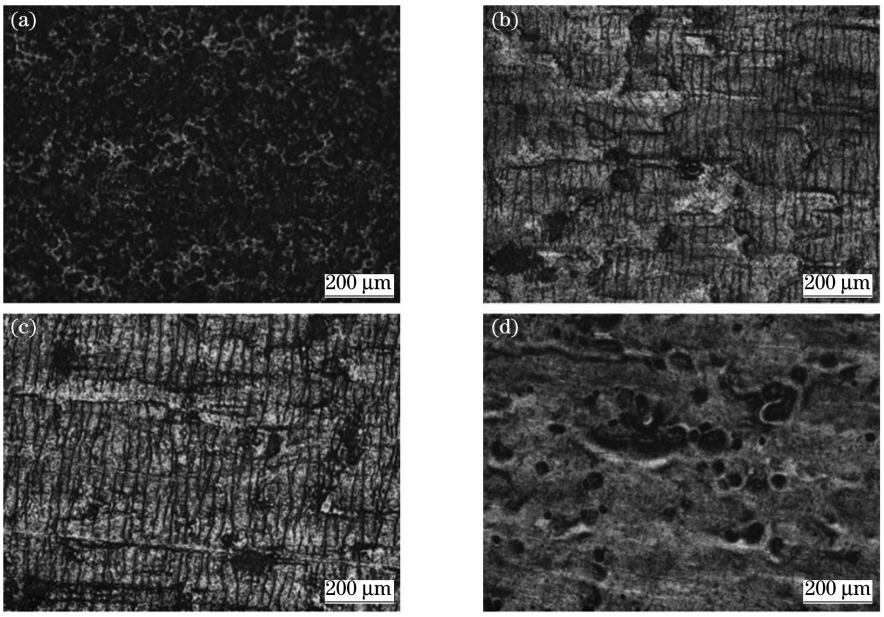

图 7 激光清洗表面微观形貌随激光功率的演变。(a) 150 W;(b) 160 W;(c)180 W;(d) 200 W

Fig. 7 Evolution of laser cleaning surface microstructures with laser power. (a) 150 W; (b) 160 W; (c) 180 W; (d) 200 W

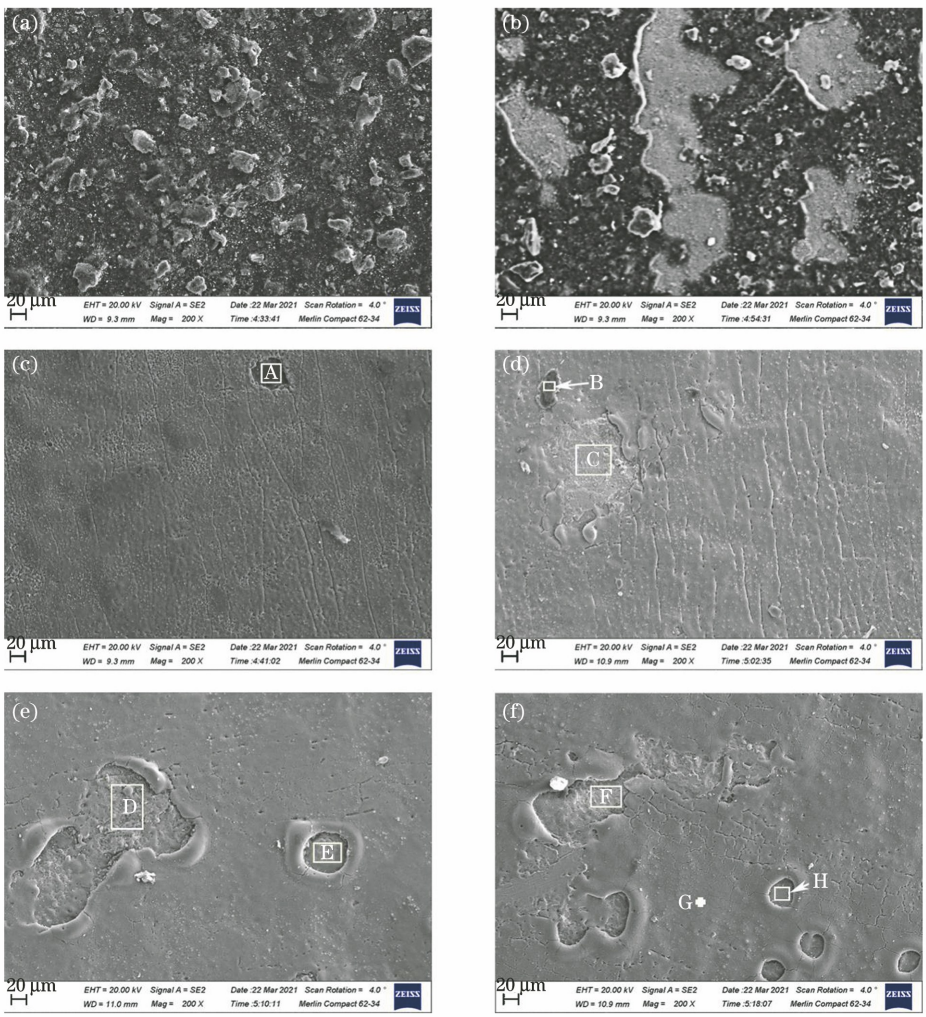

图 8 表面微观形貌。(a)150 W;(b)160 W;(c)170 W;(d)180 W;(e)190 W;(f)200 W

Fig. 8 Surface micro-morphologies. (a) 150 W; (b) 160 W; (c) 170 W; (d) 180 W; (e) 190 W; (f) 200 W

所示，表面凹坑更为密集，面积也更大，凹坑周围有明显且较为完整的火山口形貌。当激光功率达到 200 W 时，表面形貌如图 8(f)所示，表面的火山口形貌更为密集，且在凹坑处有氧化膜成片脱落的迹象。

采用扫描电镜对图 8 中各功率下的清洗表面及典型区域进行成分分析，分析结果如图 9 所示，其中碳元素含量由于系统误差而偏高，但仍可用来进行定性分析。由图 9(a)可见，原始漆层表面的碳、氧含量较高，铁含量较低。当激光功率为 150 W 时，表面的铁含量相比于原始漆层小幅增加。当激光功率增大至 160 W 时，表面的铁含量继续上升，表明基材已露出。由图 9(b)可以看出，当激光功率大于 170 W 时，表面的铁含量极高，碳含量相比原始漆层明显降低，表明此时漆层已基本被去除。同时，表面的主要元素为铁和氧，表明工件表面主要为氧化膜。

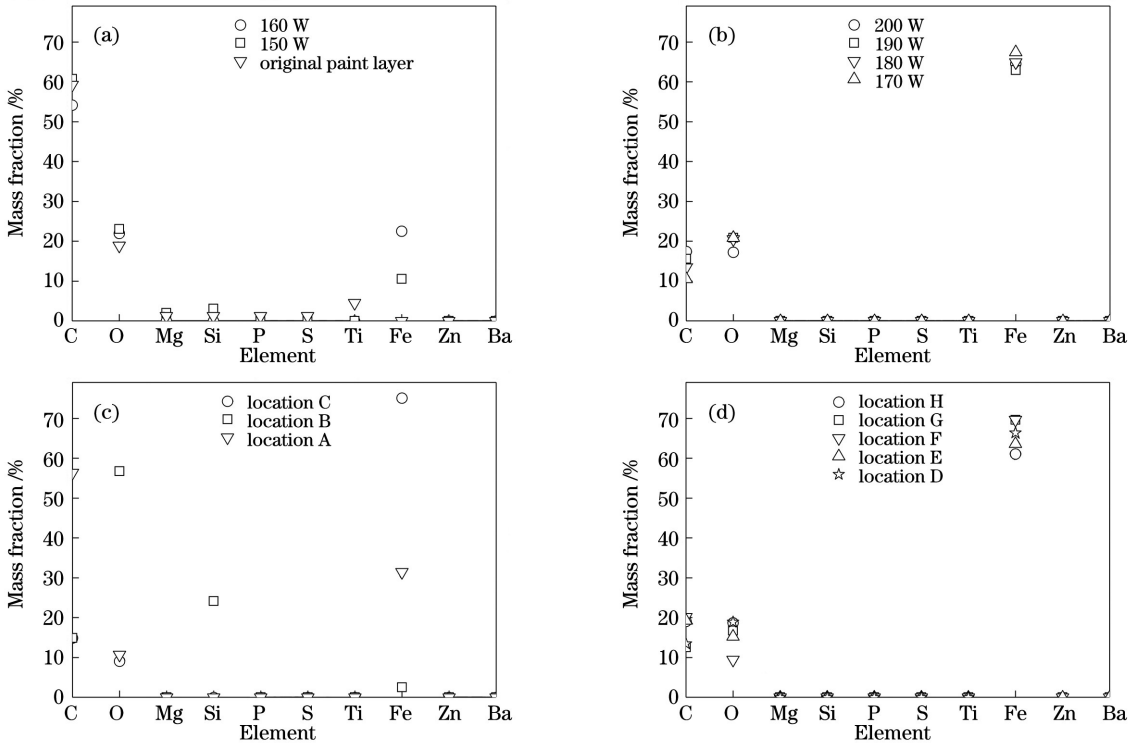

图 9 表面成分分析。(a)150～160 W 激光功率；(b)170～200 W 激光功率；(c)区域 A～C；(d)区域 D～H

Fig. 9 Surface composition analysis. (a) 150–160 W laser power; (b) 170–200 W laser power; (c) region A–C; (d) region D–H

当激光功率大于 170 W 时，工件表面逐渐出现凹坑、颗粒等缺陷。如图 9(c)所示，在 170 W 激光功率下清洗后，表面凹坑 A 中的元素组成与表层差异较大，但碳含量与原始表面相差不大。结合凹坑周围并未出现火山口等破坏性痕迹可知，该凹坑是氧化膜自身的孔洞，在涂漆时油漆填充进入凹坑中，使得清洗后凹坑中的碳含量与漆层相仿。由此可见，在 170 W 的激光功率下，涂层几乎完全被去除，且氧化膜无受损痕迹。

在 180 W 激光功率下清洗后，表面残留有区域 B 所示的颗粒状物体和区域 C 所示的凹坑。从图 9(c)所示的元素组成可以看出，B 区域表现为低铁和高氧、硅，可知颗粒是涂层中的掺入物。凹坑 C 中的铁、碳含量明显高于平均水平，且碳、氧的高含量特点与 170 W 下氧化膜缺陷内的涂层成分类似，可知其为氧化膜缺陷；凹坑 C 内的涂层清洗得更为彻底，所以铁含量更高。此外，在凹坑周围出现了局部光滑隆起，类似于不连续的火山口形貌。这说明在 180 W 的激光功率下，氧化膜有轻微的受损迹象。

由图 9(d)可见，在 190 W 激光功率下清洗后，凹坑 D、E 中的各成分与清洗表面的成分相仿。这说明这些凹坑及火山口形貌可能是氧化膜受损重熔形成的，或者是氧化膜缺陷内基材受热重熔形成的。可见，在 190 W 的激光功率下，基材均明显受损，此时清洗过度。

激光功率达到 200 W 时，F、G、H 区域的成分如图 9(d)所示。F 区中的氧含量明显低于其他区域，且凹坑右侧边缘无火山口凸起状样貌，结合氧化膜样貌突然消失这一现象可知凹坑是由氧化膜被清洗应力剥离而产生的。可见，200 W 的激光功率超

过了氧化膜的承受范围，不仅严重损伤氧化膜，甚至基体金属也受到一定损伤，此时清洗过度。

3.3　激光清洗表面的在线评估

采用在线检测装置对清洗后的表面进行扫描检测，采集的图像如图 10 所示。由图 10 可见，当将不同清洗状态的工件表面图像进行对比时，工件的面漆、底漆、金属表面及过热表面均能较为明显地区分开来。但是，当采集单一工件表面图像而缺乏对比时，则难以直接对清洗质量进行判断。因此，采用阈值法对图像进行处理，即选取对工件表面均匀性评估最为敏感的两个特征参数（方差 v_g 和平均梯度 $\bar{g}_g$）作为阈值，将这两种阈值作为判定依据。当其中任一阈值超限时，该像素单元被判定为残余漆面，像素值变更为 255（白色）；当双阈值均不超限时，该像素单元被判定为金属表面，像素值变更为 0（黑色）。图 11 是清洗表面图像的二值化处理结果。

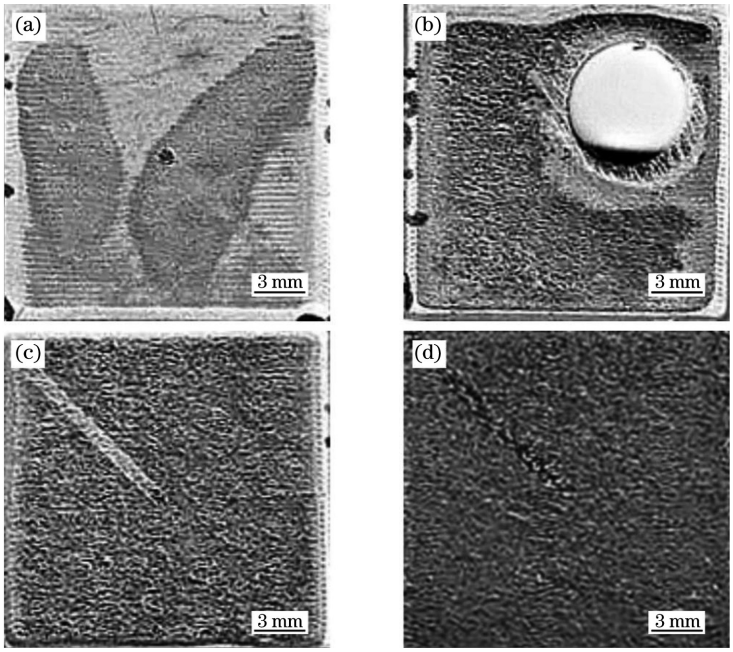

图 10　不同激光功率下的典型清洗状态图像。(a)150 W；(b)160 W；(c)180 W；(d)200 W

Fig. 10　Typical cleaning state images at different laser powers. (a) 150 W; (b) 160 W; (c) 180 W; (d) 200 W

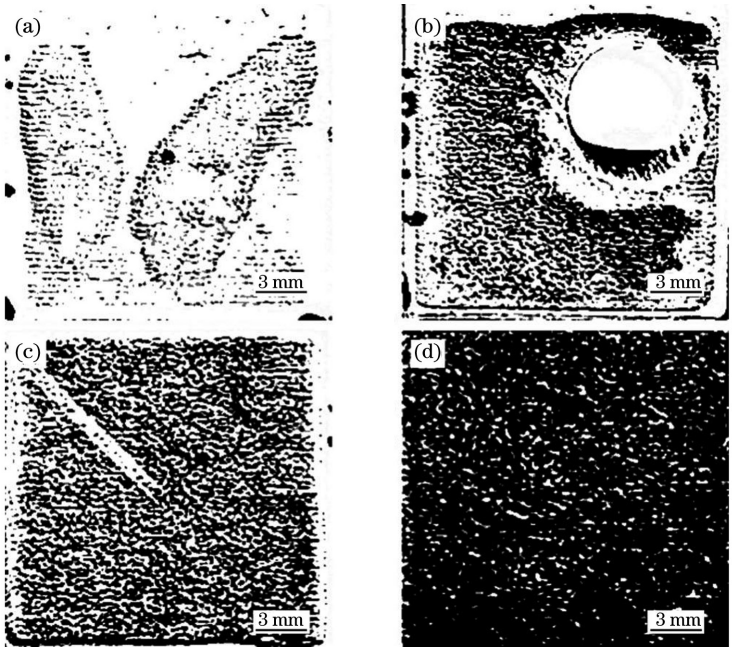

图 11　激光清洗图像的二值化处理结果。(a)150 W；(b)160 W；(c)180 W；(d)200 W

Fig. 11　Binary processing results of laser cleaning images. (a) 150 W; (b) 160 W; (c) 180 W; (d) 200 W

在图 11 中，各种清洗状态表面的区分更为容易，工件裸露的金属越多，工件清洗得越彻底，其表面黑色区域越多。将各清洗状态下二值化图像中的黑像素点和白像素点的数量进行统计，统计结果如图 12 所示。

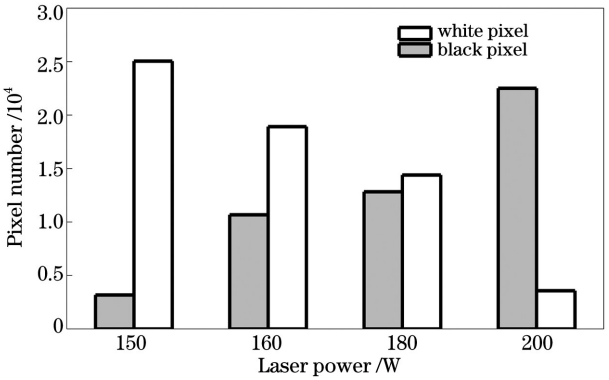

图 12 各清洗状态下黑白像素点数量的变化情况

Fig. 12 Changes in the number of black and white pixels in each cleaning state

从图 12 中可以看出，不同激光功率下清洗效果的不同反映在黑白像素点的数量上。当清洗不足时（激光功率 150 W），图像中的白色像素点数量远多于黑色像素点数量；当清洗适度时（激光功率 180 W），图像中的黑白像素点数量基本一致；当清洗过度时（激光功率 200 W），图像中白色像素点数量明显少于黑色像素点。因此，将图像中黑白像素点数量的差异作为特征值，能够直接反映漆层清洗后的残留状况。

4 结 论

采用不同参数的纳秒脉冲激光对带有漆层的试板开展激光清洗实验，对激光清洗后的表面进行宏观和微观形貌分析，得到如下结论：

1）工件表面清洗状态的宏观分析结果表明，可以根据表面颜色变化大致判断清洗程度。

2）工件表面清洗状态的微观形貌分析结果表明：当工件表面清洗不足时，漆面无烧损痕迹，表面元素主要为碳、氧和硅；当工件表面清洗适度时，表面具有清晰可见的微观氧化膜裂纹，表面元素主要为铁和氧；当工件表面过度清洗时，表面出现了明显的重熔现象，表面元素主要为铁和氧。

3）工件表面在线检测图像的二值化处理结果表明：随着清洗程度增加，图像中的白色像素点数量明显减少，黑色像素点数量明显增加；当黑色像素点数量和白色像素点数量基本一致时，表明清洗彻底。据此可以对激光清洗后的表面质量进行较为准确的评估，从而为高强钢表面漆层提供了行之有效的清洗方法和在线检测手段。

参 考 文 献

[1] Niu F J, Qi X S. Research on the application of laser cleaning technology in the maintenance of EMU[J]. China High-Tech, 2017, 1(11): 75-77.
牛富杰, 齐先胜. 激光清洗技术在动车组检修中的应用研究[J]. 中国高新科技, 2017, 1(11): 75-77.

[2] Han X H, Qi X S. Engineering application and prospect of high-efficiency and high-quality laser cleaning technology for rail passenger cars[J]. Metal Forming, 2020(3): 11-14.
韩晓辉, 齐先胜. 轨道客车高效优质激光清洗技术的工程应用与前景展望[J]. 金属加工(热加工), 2020(3): 11-14.

[3] Zhang M Q, Dai H X, Zheng Y H, et al. Research on laser cleaning detection of train paint coating based on color conversion[J]. Applied Laser, 2020, 40(4): 644-648.
张梦樵, 戴惠新, 郑云昊, 等. 基于色彩转换的列车油漆涂层激光清洗检测研究[J]. 应用激光, 2020, 40(4): 644-648.

[4] Dai H X, Zheng Y H, Luo R, et al. Research on base material properties of rail vehicle after laser cleaning paint coating[J]. Welding Technology, 2020, 49(5): 45-48.
戴惠新, 郑云昊, 罗瑞, 等. 激光清洗轨道车辆油漆涂层基材性能研究[J]. 焊接技术, 2020, 49(5): 45-48.

[5] Pozo-Antonio J S, Rivas T, Fiorucci M P, et al. Effectiveness and harmfulness evaluation of graffiti cleaning by mechanical, chemical and laser procedures on granite[J]. Microchemical Journal, 2016, 125: 1-9.

[6] Yu H B, Wang C M, Zhang W, et al. Present status and outlook of laser cleaning application development[J]. Electric Welding Machine, 2014, 44(10): 80-84.
俞鸿斌, 王春明, 张威, 等. 激光清洗应用发展现状及展望[J]. 电焊机, 2014, 44(10): 80-84.

[7] Burzic B, Hofele M, Mürdter S, et al. Laser polishing of ground aluminum surfaces with high energy continuous wave laser[J]. Journal of Laser Applications, 2017, 29(1): 011701.

[8] Kumar M, Bhargava P, Biswas A K, et al. Epoxy-paint stripping using TEA CO_2 laser: determination of threshold fluence and the process parameters[J]. Optics & Laser Technology, 2013, 46: 29-36.

[9] Lei Z L, Sun H R, Tian Z, et al. Effect of laser at

different time scales on cleaning quality of paint on Al alloy surfaces[J]. Chinese Journal of Lasers, 2021, 48(6): 0602103.
雷正龙, 孙浩然, 田泽, 等. 不同时间尺度的激光对铝合金表面油漆层清洗质量的影响[J]. 中国激光, 2021, 48(6): 0602103.

[10] Jiang G Y, Lei P, Liu Y P, et al. Laser removal of coating on oil and gas pipelines: effects on microstructure and hardness of substrate[J]. Chinese Journal of Lasers, 2020, 47(3): 0302009.
江国业, 雷璞, 刘宇平, 等. 油气管道激光除漆对基材组织和硬度的影响[J]. 中国激光, 2020, 47(3): 0302009.

[11] Guo Z H, Zhou J Z, Meng X K, et al. Nanosecond-pulsed-laser paint stripping of HT250 gray cast iron [J]. Chinese Journal of Lasers, 2019, 46(10): 1002012.
郭召恒, 周建忠, 孟宪凯, 等. HT250 灰铸铁纳秒脉冲激光除漆工艺研究[J]. 中国激光, 2019, 46(10): 1002012.

[12] Han J H, Cui X D, Wang S, et al. Laser effects based optimal laser parameter identifications for paint removal from metal substrate at 1064 nm: a multi-pulse model[J]. Journal of Modern Optics, 2017, 64(19): 1947-1959.

[13] Gao L Y, Zhou J Z, Sun Q, et al. Numerical simulation and surface morphology of laser-cleaned aluminum alloy paint layer[J]. Chinese Journal of Lasers, 2019, 46(5): 0502002.
高辽远, 周建忠, 孙奇, 等. 激光清洗铝合金漆层的数值模拟与表面形貌[J]. 中国激光, 2019, 46(5): 0502002.

[14] Majewski M S, Kelley C, Hassan W, et al. Laser induced breakdown spectroscopy for contamination removal on engine-run thermal barrier coatings[J]. Surface and Coatings Technology, 2011, 205(19): 4614-4619.

[15] Tserevelakis G J, Pozo-Antonio J S, Siozos P, et al. On-line photoacoustic monitoring of laser cleaning on stone: evaluation of cleaning effectiveness and detection of potential damage to the substrate [J]. Journal of Cultural Heritage, 2019, 35: 108-115.

[16] Tserevelakis G J, Pouli P, Zacharakis G. Listening to laser light interactions with objects of art: a novel photoacoustic approach for diagnosis and monitoring of laser cleaning interventions[J]. Heritage Science, 2020, 8(1): 1-13.

[17] Chen Y, Deng G L, Zhou Q H, et al. Acoustic signal monitoring in laser paint cleaning[J]. Laser Physics, 2020, 30(6): 066001.

[18] Xie X Z, Huang Q P, Long J Y, et al. A new monitoring method for metal rust removal states in pulsed laser derusting via acoustic emission techniques[J]. Journal of Materials Processing Technology, 2020, 275: 116321.

[19] Papanikolaou A, Tserevelakis G J, Melessanaki K, et al. Development of a hybrid photoacoustic and optical monitoring system for the study of laser ablation processes upon the removal of encrustation from stonework [J]. Opto-Electronic Advances, 2020, 3(2): 190037.

Quality Analysis and Online Evaluation of Axle Surface After Laser Cleaning

Wang Chunsheng[1], Wang Hongxiao[1], Xu Huiyan[2], He Guangzhong[1], Li Kai[1], Gu Xiaopeng[2], Dong Juan[2*]

[1] *Engineering and Technology Center, CRRC Changchun Railway Vehicles Co., Ltd., Changchun, Jilin* 130113, *China*;
[2] *College of Materials Science and Engineering, Jilin University, Changchun, Jilin* 130112, *China*

Abstract

Objective The main component of high-speed rail is the bogie wheel, which has extremely strict maintenance requirements. The surface coating needs to be removed in advanced maintenance. Traditional surface coating removal methods are mechanical grinding and chemical treatment. These methods can easily cause excessive grinding in local areas, thereby causing surface damage. Therefore, designing a new coating removal technology is urgent to reduce environmental pollution, labor costs and achieve green, efficient, and high-quality coating removal. Laser cleaning technology has been widely used in coating surface treatment because of its high cleaning accuracy with no chemical cleaning agent and no physical or mechanical contact. Moreover, it can be easily automated. Therefore, we

adopt laser cleaning technology for the axle body of existing high-speed rail bogie wheel sets. Through the laser cleaning process analysis of the surface coating of high-strength steel, the evolution of the surface microstructure of high-strength steel after laser cleaning, and the online evaluation method of the surface quality after laser cleaning, a breakthrough is made in the laser cleaning technology of the surface of a high-strength steel axle. Thus, it lays the application foundation for applying green and efficient surface treatment technology to overhaul key parts of the high-speed railway body.

Methods High-strength steel was chosen as the experimental material, and red primer and gray finish were sprayed on the surface. The primer thickness was 50–60 μm, and the gray finish thickness was 230–260 μm. During laser cleaning experiment, laser was used to scan the sample surface along the bow-shaped path. The main laser cleaning process parameters were listed in Table 2. The surface morphology and composition of the prepared samples were observed and analyzed using the laser confocal microscope, digital microscope, and field emission scanning electron microscope. The experimental design of the laser cleaning workpiece surface inspection mechanism and laser cleaning quality was evaluated.

Results and Discussions Macroscopic morphology analysis (Fig. 5) shows that the paint removal rate gradually increases as the laser power increases. For instance, at 70 W, only part of the top paint can be removed, and the surface is smooth and light gray. At 150 W, the finish paint can be removed, and the surface is jujube red. When the laser power reaches 200 W, the paint layer can be roughly removed, and the silvery metal surface can be exposed. Under the optical microscope, there are gully cracks on the surface of high-strength steel. At 240 W, the surface is blue and purple after excessive cleaning, indicating ablation.

Microscopic appearance analysis (Figs. 6–8) shows that when the laser power is 150 W, the primer surface has no scorch mark and the surface is not smooth. Additionally, the stripping mechanism plays a dominant role. Meanwhile, when the laser power is 160 W, the oxide film on the surface of the substrate can be exposed, whereas a large amount of primer remains on the surface of the substrate. The cracks on the oxide film are more clearly visible when the laser power is 180 W; however, sporadic remelting appeared in the weak part of the oxide film. Furthermore, the edge of the oxide film crack appears passivation when the laser power is 200 W; the crater-like remelting appears, and the substrate is slightly damaged.

The following results were obtained from the composition analysis (Fig. 9). The original paint surface contains high C and O contents and low Fe content. The Fe content on the surface increases slightly when the laser power is 150 W. Meanwhile, the Fe content on the surface increases when the laser power becomes 160 W, indicating that the substrate has been exposed. The main elements on the surface when the laser power is greater than 170 W are Fe and O, indicating that the surface of the workpiece is mainly oxide film. The workpiece surface with laser power of 170 W gradually exposes the oxide film holes that exist on the oxide film, and the oxide film has no trace of remelting damage. At 180 W laser power, the surface had residual additives in the coating, and the oxide film is slightly damaged. At 190 W laser power, the oxidation film on the surface is damaged and remelted to form pits. When the laser power reaches 200 W, the pits on the surface are caused by the stripping of the oxide film in laser cleaning process, indicating that the internal metal is damaged.

An online detection device shown in Fig. 4 was used to scan and detect the surface of the cleaned workpiece. The online detection device uses a precision motion module to drive a camera to scan the workpiece for collecting surface information. The analysis results of the collected images using double thresholds (Fig. 12) show that the difference in cleaning effects has evident characteristics in the number of black/white pixels. When cleaning is insufficient (laser power of 150 W), the number of white pixels in the image is much higher than that of black pixels. Meanwhile, when cleaning is moderate (laser power of 180 W), the number of black and white pixels in the image is almost the same. Furthermore, for excessive cleaning (laser power of 200 W), the number of white pixels in the image is substantially lower than that of black pixels. Therefore, the difference between the number of black and white pixels in the image can be considered as the characteristic value, reflecting the cleaning residue status of the coating.

Conclusions Nanosecond pulse laser with different parameters was used to conduct laser cleaning experiments. Macroscopic and microscopic morphologies of the surfaces after laser cleaning were analyzed, and their properties were studied. The following conclusions were obtained. Macroscopic analysis of workpiece surface cleaning state shows that when the paint layer is insufficient or excessive cleaning, the cleaning degree can be roughly judged according to the change of surface color. The microstructure analysis of the workpiece surface cleaning state shows no burning trace on the paint surface when the workpiece surface cleaning is insufficient, and the surface elements

are mainly C, O, and Si. Meanwhile, when the workpiece surface cleaning is moderate, the surface has visible microscopic oxide film cracks, and the surface elements are mainly Fe and O. Furthermore, the surface has an evident remelting phenomenon when the workpiece surface is overcleaned, and the surface elements are mainly Fe and O. The binarization processing results show that with an increase in cleaning degree, the number of white pixels in the image decreases, whereas the number of black pixels increases. Moreover, when the number of black and white pixels is almost the same, the cleaning is complete. According to this method, the surface quality after laser cleaning can be accurately evaluated. Our study provides an effective cleaning method and testing means for the surface paint film of the bogie wheel of high-speed rail.

Key words laser technique; laser cleaning; surface appearance; laser ranging; online assessment